High Power Laser Science and Engineering, (2020), Vol. 8, e32, 6 pages.
doi:10.1017/hpl.2020.32

HIGH POWER LASER SCIENCE AND ENGINEERING

LETTER

Mid-infrared optical frequency comb in the 2.7–4.0 μm range via difference frequency generation from a compact laser system

Lian Zhou[1], Yang Liu[1], Gehui Xie[1], Chenglin Gu[1], Zejiang Deng[1], Zhiwei Zhu[1], Cheng Ouyang[1], Zhong Zuo[1], Daping Luo[1], Bin Wu[3], Kunfeng Chen[3], and Wenxue Li[1,2]

[1]*State Key Laboratory of Precision Spectroscopy, East China Normal University, Shanghai 200062, China*

[2]*Collaborative Innovation Center of Extreme Optics, Shanxi University, Taiyuan 030006, China*

[3]*Science and Technology on Electronic Test & Measurement Laboratory, The 41st Research Institute of CETC, Qingdao 266000, China*

(Received 4 June 2020; revised 11 July 2020; accepted 5 August 2020)

Abstract

We report on the generation of a mid-infrared (mid-IR) frequency comb with a maximum average output power of 250 mW and tunability in the 2.7–4.0 μm region. The approach is based on a single-stage difference frequency generation (DFG) starting from a compact Yb-doped fiber laser system. The repetition rate of the near-infrared (NIR) comb is locked at 75 MHz. The phase noise of the repetition rate in the offset-free mid-IR comb system is measured and analyzed. Except for the intrinsic of NIR comb, environmental noise at low frequency and quantum noise at high frequency from the amplifier chain and nonlinear spectral broadening are the main noise sources of broadening the linewidth of comb teeth, which limits the precision of mid-IR dual-comb spectroscopy.

Keywords: fiber laser; mid-infrared; optical frequency comb

1. Introduction

Mid-infrared (mid-IR) laser sources are now becoming enabling tools for cutting-edge applications, including greenhouse gas sensing[1, 2], medical diagnosis[3], and security and defense[4]. Many molecules and molecular functional groups experience vibrational absorption in the mid-IR region. Indeed, spectroscopic applications would benefit from scaling the optical frequency comb to the mid-IR region, leading to numerous absorption lines being recorded with unprecedented accuracy and resolution[5, 6]. Moreover, ultrafast pulses with a stable carrier–envelope phase permit an exhaustive understanding of molecular structure and dynamics[7, 8], and they enable the soft X-ray generation to be scaled on a tabletop system[9, 10]. Over the last decade, steady progress has been made in the field of ultrafast mid-IR frequency comb generation. There is a wide array of innovative solutions to generate coherent mid-IR laser sources, with novel gain media[11], quantum cascade lasers[12] and micro-resonators[13], and supercontinuum generation in waveguides and fibers[14, 15]. Compared with these approaches, detecting and controlling the offset frequency of the mid-IR sources is a challenge, which is the prerequisite for frequency comb spectroscopy. A more direct approach is to employ nonlinear frequency conversion of ultrashort pulses in the visible or near-infrared (NIR) regime to generate coherent mid-IR sources. Among the different nonlinear processes, difference frequency generation (DFG) with signal and pump from the same oscillator offers several advantages for a mid-IR frequency comb system, as it allows us to use compact and well-developed fiber laser technology, and also to achieve ultrashort pulses and intrinsic carrier–envelope phase stability, which reduce the complexity and improve the quality of the long-term performance[16–19]. In DFG systems, the mid-IR spectrumd coverage depends on the NIR spectrum and the transmissivity of the crystal. Limited by the gain bandwidth of laser materials, the general NIR sources cannot directly emit pulses with such a broad spectrum. To achieve a broad mid-IR spectrum, highly

Correspondence to: W. Li and Y. Liu, No. 500 Dongchuan Road, Shanghai 200241, China. Email: wxli@phy.ecnu.edu.cn (W. Li); yliu@lps.ecnu.edu.cn (Y. Liu)

nonlinear fiber (HNLF) is widely applied in DFG systems for NIR spectrum broadening. The oscillators split the output laser into two beams and nonlinearly broaden the NIR laser in HNLF[16–20]. By phase matching, the signal and pump pulses are focused into a crystal to generate an idler pulse in the mid-IR region. The latest representative work demonstrated a high-power mid-IR femtosecond source with a broad spectrum from 1.6 to 10.2 μm by DFG[21]. With such a broad spectrum, the high-power mid-IR femtosecond source will be a powerful tool for multispecies trace gas detection.

Benefitting from the development of dual-comb technology, high-speed comb-tooth-resolved broadband mid-IR dual-comb spectroscopy (DCS) has been presented[6, 22]. In a dual-comb system, a narrow linewidth of the comb teeth is expected for high-resolution DCS. The linewidth of the mid-IR comb generated by DFG is related to the phase noise of the NIR source. Compared with mid-IR combs, NIR combs are better at measuring and controlling phase noise. The noise of the mid-IR comb can be controlled by locking the repetition rate (f_r) of the NIR comb. Therefore, the low phase noise of two NIR sources is fundamental to achieve high-resolution DCS. Although various ultralow-noise NIR oscillators have been demonstrated[23], excess phase noise from the NIR amplification and DFG process will lead to linewidth broadening of the mid-IR comb.

In this letter, we report on a mid-IR comb based on an NIR system. The NIR system includes an Yb:fiber comb and an Yb fiber chirped pulse amplifier (CPA) emits a pulse train with a 4 W average power and a 194 fs pulse duration. The NIR source is spilt into two beams as the signal and pump pulses of DFG. The spectrum of the signal pulse is nonlinearly broadened in a piece of HNLF with anomalous dispersion. The pump and signal pulses are focused into periodically poled lithium niobate (PPLN) for DFG. The mid-IR comb has a tunable spectrum from 2.7 to 4.0 μm and a maximum average power of 250 mW. To confirm the noise source, we measured the noise of each module and analyzed the noise source. This work has the potential to develop low-noise mid-IR combs, which may be applied in high-coherence DCS.

2. Experimental setup

The schematic representation of the mid-IR frequency comb is shown in Figure 1. The front end of the mid-IR frequency comb is combined by an all-polarization-maintaining fiber oscillator and a chirped pulse fiber amplifier. The Yb:fiber oscillator serves as the NIR comb, the repetition rate (f_r) of which is locked to a Rb-clock at 75 MHz and the carrier–envelope offset (f_0) is free-running. The power amplifier relies on chirped pulse amplification consisting of a 100 m fiber stretcher and two-stage amplifiers, which operate in gain-saturation state to reduce the amplified spontaneous emission (ASE), and delivers 89 nJ energy pulses centered at 1038 nm. A grism pair with a 60% efficiency compensates for the group delay dispersion and third-order dispersion, leading to 152 fs dechirped pulses. Then, the compressed NIR pulse train is spilt into two arms as the signal and pump laser. The signal laser is coupled into a highly nonlinear photonic crystal fiber (PCF) with 26 nJ pulse energy. A 16 cm long highly nonlinear PCF was used to broaden the spectrum. This highly nonlinear PCF (NL-3.3-890) with a zero-dispersion wavelength at 890 nm provides anomalous dispersion to the signal laser. The nonlinear broadening process is sensitive to the pulse energy and polarization of the input NIR laser. Therefore, a half-wavelength plate and an attenuation filter are placed in front of the fiber to optimize the spectrum of the signal laser. Polarization of the signal laser is adjusted by another half-wavelength plate after nonlinear broadening, which contributes to optimizing the conversion efficiency of DFG. After propagating through an optical delay line, the pump laser is combined with

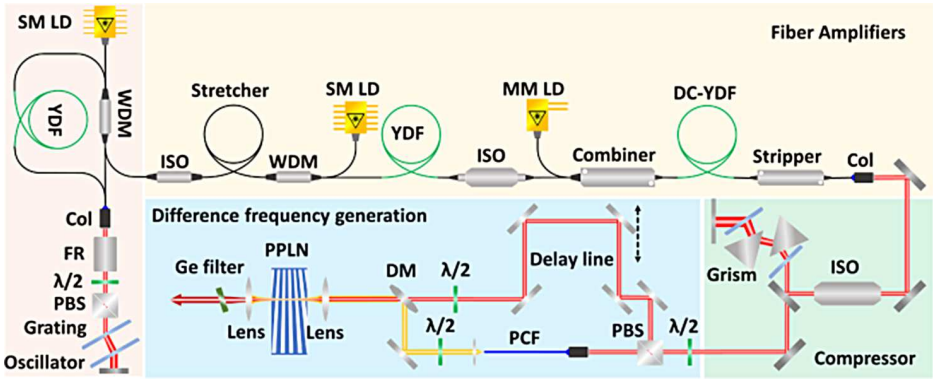

Figure 1. Schematic of the mid-IR comb. The mode-locked fiber oscillator serves as an NIR comb whose repetition rate is locked at 75 MHz. The CPA with two-stage fiber amplifiers scales the average power to 6.7 W. After the compressor, the system emits a pulse train with an average power of 4 W and a pulse duration of 194 fs, which corresponds to a pulse energy of 53 nJ. In the DFG module, the mid-IR pulse laser is generated in the PPLN by quasi-phase matching. SM LD, single-mode laser diode; YDF, Yb-doped fiber; WDM, wavelength division multiplexer; Col, collimator; FR, Faraday rotator; PBS, polarization beam splitter; ISO, isolator; MM LD, multimode laser diode; DC-YDF, double-cladding Yb-doped fiber; PCF, photonic crystal fiber; DM, dichroic mirror; PPLN, periodically poled lithium niobate.

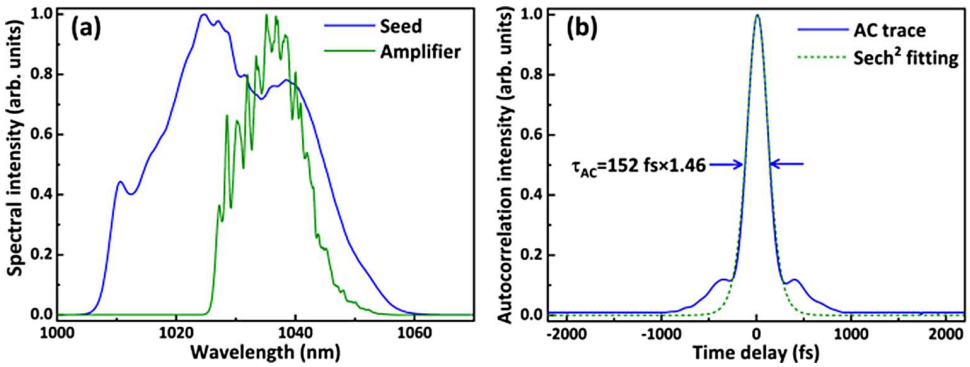

Figure 2. Characterization of the chirped pulse amplification. (a) Normalized optical spectrum of NIR oscillator (blue curve) and amplified pulse (green line), centered at 1030 and 1038 nm with a spectral width of 30 and 12 nm, respectively. (b) Measured autocorrelation trace (blue line) of the amplified pulse with corresponding sech fitting (dotted green line).

the broadened signal laser by a dichroic mirror. Using an achromatic lens with a focal length of 50 mm, the signal and pump pulses are focused into a 25 mm long PPLN crystal for quasi-phase matching. The generated mid-IR idler laser is collimated by a CaF_2 lens and separated by a long-pass filter.

3. Results and discussion

The NIR ultrafast pulse source is a home-made PM Yb-doped fiber laser based on a nonlinear amplifying loop mirror. By tuning the intracavity grating pair, the net dispersion of the cavity is controlled to near zero for low intrinsic phase noise[24]. The laser emits 3 mW pulses with 30 nm full width at half maximum (FWHM) and 75 MHz repetition rate. As this pulse energy is insufficient for broad signal laser generation, CPA is employed to scale pulse energy. Before spectral broadening, the NIR pulse is coupled into a section of PM fiber for pulse duration stretching. After amplification, the seed spectral bandwidth is narrowed to less than 15 nm under the action of gain narrowing, as shown in Figure 2(a). The group delay and third-order dispersion accumulated in stretcher and fiber amplifiers are compensated by a grism pair. The detailed design and structure are described in Ref. [25]. At 4 W average power, the dechirped pulse has a temporal width of 152 fs as shown in Figure 2(b). The autocorrelation trace of the compressed pulses shows small distortions from the sech shape.

The amplified high-power pulses were split into two branches by a half-wave plate and a polarization beam splitter. The signal branch with a pulse energy of 26 nJ was coupled into a highly nonlinear PCF to broaden the spectrum. The length of PCF was chosen as 16 cm to obtain high coherence of Raman solitons. By optimizing the polarization and average power of the signal pulse, a broadened signal laser with spectral coverage from 1.1 to 1.6 mm (there is a weak component at 1.7 μm, the detected wavelength coverage of Yokogawa AQ6370 optical spectrum analyzer is 600–1700 nm) is achieved, as shown in Figure 3(a). The pump branch centered at 1038 nm with pulse energy of 26 nJ passed through a delay line stage to control the temporal overlap of signal and pump pulses. The signal and pump lasers were spatially combined by a longwave-reflective dichroic mirror and then were focused into a 25 mm long MgO:PPLN with 10 mol% MgO doping (CTL Photonics). The MgO:PPLN crystal designed with six channels ensures variable periods from 28.0 to 30.5 μm.

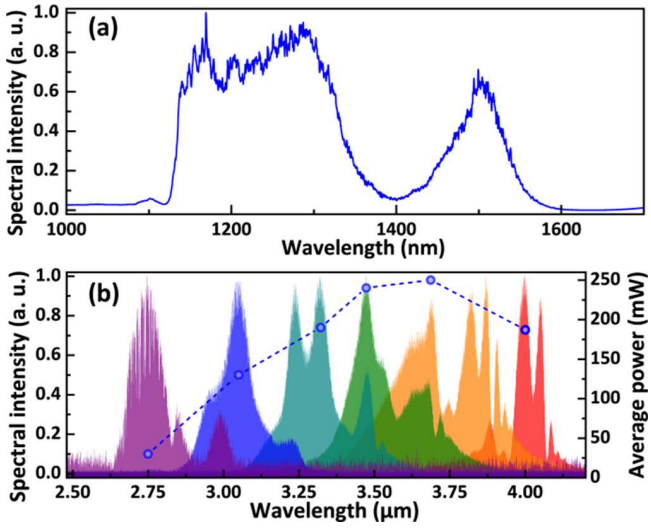

Figure 3. (a) The spectrum of the broadened signal laser after a long-pass filter at 1100 nm. (b) The spectrum and corresponding average power of the mid-IR comb. The mid-IR comb has a tunable coverage of 2.7–4.0 μm. The average powers are 30, 130, 190, 240, 250, and 187 mW centered at 2.7, 3.0, 3.3, 3.5, 3.7, and 4.0 μm, respectively.

We optimize the conversion efficiency of quasi-phase matching by adjusting the optical delay line. The mid-IR comb is collimated by an uncoated CaF_2 lens with a focal length of 75 mm. A 3 mm thick Ge filter separates the mid-IR comb from the pump and signal lasers. The spectral, temporal, long-term frequency stabilization and phase noise performances were measured to characterize

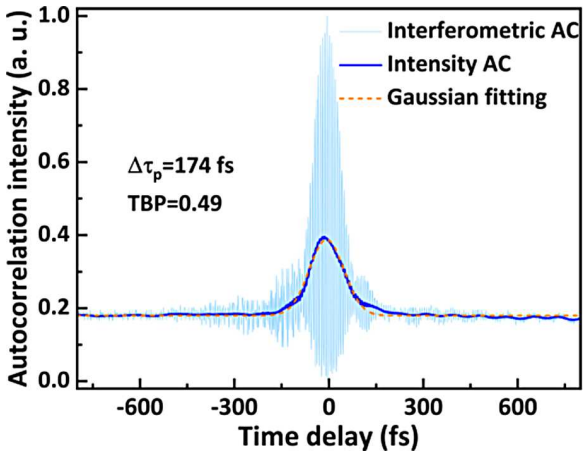

Figure 4. The autocorrelation of mid-IR pulse at 3.5 μm. The pulse duration is 174 fs with Gaussian fitting.

the mid-IR comb. The spectral coverage of the mid-IR comb was measured by a Fourier transform spectrometer as shown in Figure 3(b). The obtained tunable spectrum from 2.7 to 4.0 μm is obtained by tuning the poling period of the PPLN at fixed pump and signal laser power. The short-wavelength extension is blocked at 2.7 μm, which is limited by the longest signal wavelength generation from the PCF. A series of absorption lines in this spectrum are caused by water vapor in laboratory air (relative humidity ~45%, optical path length ~1 m). The maximum average output power is limited to 30 mW owing to a weak signal laser at 1.7 μm. Adjusting the PPLN channel to the poling period of 30.0 μm, the central wavelength can be tuned to 3.1 μm with an output power of 130 mW and an FWHM of 200 nm. With decreasing poling periods, a higher output power and a broader spectral bandwidth can be achieved. The maximum output power is 250 mW, which is obtained at a central wavelength of 3.7 μm with an FWHM of 300 nm. The longest wavelength we can achieve is limited by the poling period (28.0 μm) and increasing absorption of the crystal at long wavelength (>1 cm^{-1} when the wavelength >4.0 μm).

The temporal profile of the mid-IR pulse at 3.5 μm was measured by a homemade interferometric autocorrelator based on a two-photon absorption detector. The interferometric autocorrelation trace is shown in Figure 4, which is deconvolved by a factor of 0.774 with a width of 246 fs, corresponding to a 174 fs pulse duration fitted with Gaussian shape. The pulse time–bandwidth product is 0.49 indicating the pulse is close to the bandwidth-limited value (0.44 for a Gaussian pulse).

In the DFG process, the f_0 of the mid-IR pulse is stabilized passively. To stabilize the f_r of the mid-IR comb, we locked the f_r of the NIR comb by driving an intracavity piezoelectric transducer (PZT). A home-made InGaAs detector and a HgCdTe detector (VIGO, PCI-10.6-1×1) were used to detect the NIR and mid-IR signal. After detecting the signal, we adjusted this microwave signal power at –10 dBm with an optical attenuator. Then a commercial phase noise analyzer (R&S, FSWP8) was used to measure the phase and amplitude noise. The phase noise of the repetition rate is shown in Figure 5(a). By isolating environmental perturbations and driving the PZT, the phase noise of the NIR comb at 1 Hz is suppressed to –86 dBc/Hz. However, the vibration of PZT brings intracavity environmental perturbations, which result in a peak of –93 dBc/Hz at 74 Hz. The integrated phase noise from 10 MHz to 1 Hz of the NIR comb is 0.188 mrad. After the CPA, the phase noise has an obvious increase at 1–30 Hz. The main cause, which leads to the deterioration of phase noise in the low-frequency region, is environmental perturbations to the long-path amplification system. From 1 kHz to 10 MHz, the phase noise is attenuated because of the reduction of ASE-induced quantum limited noise[26], which is beneficial to gain saturation amplification in the CPA. The amplified laser has a low integrated phase noise of 0.272 mrad. In contrast, the mid-IR comb has a degradation with an integrated phase noise of 3.230 mrad. In the frequency range of 1–20 Hz, environmental perturbations lead to a small increase of low-frequency noise. The noise curve of mid-IR comb expresses a coincidence with the noise curve of the amplified NIR laser at 20–400 Hz. However, the phase noise of mid-IR laser becomes seriously degraded at 400 Hz–10 MHz. The 'flat' phase noise at 400 Hz–10 MHz is caused mainly by the supercontinuum generation and the shot noise of the mid-IR detector. The ASE from the oscillator and amplifier, which results in the increase of quantum-limited noise, brings excess phase noise in the HNLF. The increase of ASE-induced quantum limited noise leads a 'flat' noise curve to the signal pulse at 400 Hz–1 MHz[26, 27]. The excess phase noise is transmitted to the mid-IR pulse after DFG. The shot noise of the mid-IR detector results in a weak increase of phase noise at 1–10 MHz because of the signal-to-noise ratio limit of the mid-IR pulse.

Figure 5(b) shows the relative intensity noise (RIN) of the NIR comb, CPA, and mid-IR comb: the integrated RINs from 10 MHz to 1 Hz are 0.0076%, 0.1351%, and 3.9980%, respectively. It is demonstrated that saturation amplification will lead to an attenuation in the frequency range of 1 Hz–10 kHz[28]. The RIN is not attenuated at low frequency in this CPA operating at saturation amplification. Therefore, the environmental perturbations (1–30 Hz) and pump noise (30 Hz–10 kHz) are the dominant noise sources, which cause a strong increase of RIN and offset the attenuation caused by saturation amplification. ASE and shot noise are the main noise sources at high frequency (10 kHz–10 MHz). After DFG, the obtained RIN of the mid-IR comb expresses a serious degradation with an integrated RIN of 3.9980%. The intensity noise of the input pulse will be amplified in the supercontinuum generation, the spectral broadening of which is sensitive to the peak power of the initial pulse[29, 30]. The intensity noise caused

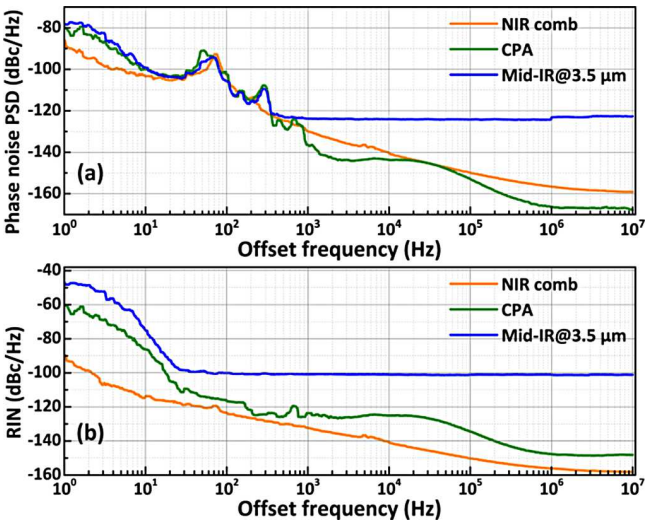

Figure 5. (a) Phase noise PSD and (b) relative intensity noise (RIN) of the repetition rate signal corresponding to NIR comb (origin), CPA (green), and mid-IR comb at 3.5 μm (blue).

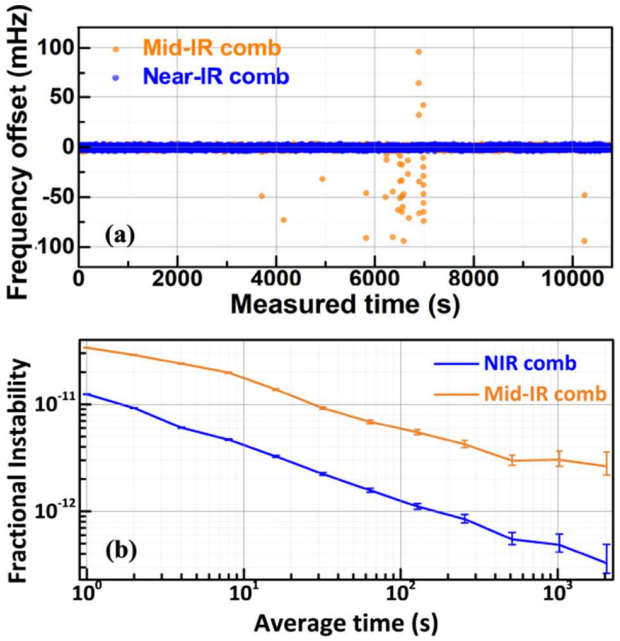

Figure 6. (a) The measured repetition rate stability of NIR comb (blue) and mid-IR comb (orange) for 3 h. (b) The Allan variance of the NIR comb (blue) and mid-IR comb (orange).

by unstable supercontinuum generationat low frequency is transmitted from the signal pulse to the mid-IR pulse. Moreover, environmental perturbations lead to a random time delay between the signal and pump pulses, which results in a random power instability to the mid-IR pulse. Silva de Oliveira *et al*.[31] demonstrated that RIN is related to the temporal overlap in a DFG process, and the lowest RIN is obtained when the pump and signal pulses have no delay. Therefore, the mid-IR comb with free-running pump–signal delay has higher environmental noise in the low-frequency region. Therefore, the excess RIN at 1 Hz–1 kHz is related to the supercontinuum generation and environmental perturbations. The 'flat' RIN curve at 1 kHz–10 MHz is related to the quantum noise sources including broadband shot noise and the spontaneous Raman scattering[29].

Therefore, the phase noise sources in this system are the environmental noise at low frequency and ASE-induced quantum noise at high frequency from the amplifier chain and nonlinear spectral broadening. The RIN sources are the environmental noise, pump noise of the amplifier, unstable supercontinuum generation, and quantum noise. For further applications in high-coherence DCS, the feedback control system, environmental isolation, power fluctuations of the pump laser, ASE suppression, and spectrum broadening need to be improved to reduce the phase noise of the mid-IR comb.

To test the long-term frequency stabilization of the mid-IR comb, the frequency fluctuation of the repetition rate was first detected by a thermoelectrically cooled photodetector (PVI-4TE-10.6, VIGO). Subsequently, the repetition rate signal after an electronic bandpass filter centered at 75 MHz was recorded by a ∧-type counter, which was referenced to the same Rb-clock for the NIR comb. The frequency fluctuations of the NIR comb were measured simultaneously to compare and calibrate the mid-IR comb. The recorded frequency fluctuations with a measurement time of 3 h are shown in Figure 6(a). The mid-IR comb has more significant frequency fluctuations, the main cause of which is power instability detected by the mid-IR photodetector in our opinion. The recorded data of repetition rate fluctuations were limited by the counter we used: the corresponding resolution was 0.375 mHz at 1 s gate time. The standard deviations were 1.26 and 3.54 mHz, respectively. The Allan variances were 1.24×10^{-11} and 3.32×10^{-11} at 1 s, as shown in Figure 6(b). The NIR comb and mid-IR comb have a good performance in long-term stability.

4. Conclusions

A mid-IR comb with tunable spectrum from 2.7 to 4.0 μm has been achieved by DFG. The maximum average power is 250 mW, which has been obtained at a central wavelength of 3.7 μm with an FWHM of 300 nm. By controlling the frequency and optimizing this system structure, this mid-IR comb system exhibits long-term frequency stability. The phase noise source has been analyzed by comparing the noise variation of Yb:fiber comb, CPA module, and mid-IR comb. Except for the intrinsic phase noise of the NIR comb, environmental noise at low frequency and quantum noise at high frequency from the amplifier chain and nonlinear spectral broadening are the additional noise source. Further measures, which consist of a precise feedback control

system, good environmental isolation, suppression of the ASE, and so forth, will be taken to develop low-noise mid-IR combs in our future work for high-resolution spectroscopy in the mid-IR region.

Acknowledgments

This work was partially supported by the National Natural Science Foundation of China (Nos. 11804096, 11874153, and 11904105), the National Key R&D Program of China (Nos. 2018YFA0306301 and 2017YFF0206000), and the Shanghai Sailing Program (No. 18YF1407300).

References

1. J. Mulrooney, J. Clifford, C. Fitzpatrick, and E. Lewis, Sens. Actuator A Phys. **136**, 104 (2007).
2. J. J. Scherer, J. B. Paul, H. J. Jost, and M. L. Fischer, Appl. Phys. B **110**, 271 (2013).
3. M. J. Thorpe, D. B. Clausen, M. S. Kirchner, and J. Ye, Opt. Express **16**, 2387 (2008).
4. A. Tsekoun, A. Lyakh, R. Maulini, M. Lane, T. Macdonald, R. Go, C. Kumar, and N. Patel, Proc. SPIE **7325**, 73250L (2009).
5. A. V. Muraviev, V. O. Smolski, Z. E. Loparo, and K. L. Vodopyanov, Nat. Photonics **12**, 209 (2018).
6. G. Ycas, F. R. Giorgetta, E. Baumann, I. Coddington, D. Herman, S. A. Diddams, and N. R. Newbury, Nat. Photonics **12**, 202 (2018).
7. D. Mathur, K. Dota, A. K. Dharmadhikari, and J. A. Dharmadhikari, Phys. Rev. Lett. **110**, 083602 (2013).
8. B. Piglosiewicz, S. Schmidt, D. J. Park, J. Vogelsang, P. Groß, C. Manzoni, P. Farinello, G. Cerullo, and C. Lienau, Nat. Photonics **8**, 37 (2014).
9. T. Popmintchev, M.-C. Chen, D. Popmintchev, P. Arpin, S. Brown, S. Alisauskas, G. Andriukaitis, T. Balciunas, O. D. Mucke, A. Pugzlys, A. Baltuska, B. Shim, S. E. Schrauth, A. Gaeta, C. Hernandez-Garcia, L. Plaja, A. Becker, A. Jaron-Becker, M. M. Murnane, and H. C. Kapteyn, Science **336**, 1287 (2012).
10. T. Popmintchev, M.-C. Chen, P. Arpin, M. M. Murnane, and H. C. Kapteyn, Nat. Photonics **4**, 822 (2010).
11. R. I. Woodward, D. D. Hudson, A. Fuerbach, and S. D. Jackson, Opt. Lett. **42**, 4893 (2017).
12. Q. Y. Lu, M. Razeghi, S. Slivken, N. Bandyopadhyay, Y. Bai, W. J. Zhou, M. Chen, D. Heydari, A. Haddadi, R. McClintock, M. Amanti, and C. Sirtori, Appl. Phys. Lett. **106**, 051105 (2015).
13. M. Yu, Y. Okawachi, A. G. Griffith, N. Picqué, M. Lipson, and A. L. Gaeta, Nat. Commun. **9**, 1869 (2018).
14. B. Kuyken, T. Ideguchi, S. Holzner, M. Yan, T. W. Hänsch, J. Van Campenhout, P. Verheyen, S. Coen, F. Leo, R. Baets, G. Roelkens, and N. Picqué, Nat. Commun. **6**, 6310 (2015).
15. T. Cheng, K. Nagasaka, T. H. Tuan, X. Xue, M. Matsumoto, H. Tezuka, T. Suzuki, and Y. Ohishi, Opt. Lett. **41**, 2117 (2016).
16. T. W. Neely, T. A. Johnson, and S. A. Diddams, Opt. Lett. **36**, 4020 (2011).
17. T. A. Johnson and S. A. Diddams, Appl. Phys. B. **107**, 31 (2012).
18. F. C. Cruz, D. L. Maser, T. Johnson, G. Ycas, A. Klose, F. R. Giorgetta, I. Coddington, and S. A. Diddams, Opt. Express **23**, 26814 (2015).
19. D. L. Maser, G. Ycas, W. I. Depetri, F. C. Cruz, and S. A. Diddams, Appl. Phys. B **123**, 142 (2017).
20. G. Soboń, T. Martynkien, P. Mergo, L. Rutkowski, and A. Foltynowicz, Opt. Lett. **42**, 1748 (2017).
21. M. Seidel, X. Xiao, S. A. Hussain, G. Arisholm, A. Hartung, K. T. Zawilski, P. G. Schunemann, F. Habel, M. Trubetskov, V. Pervak, O. Pronin, and F. Krausz, Sci. Adv. **4**, 1526 (2018).
22. G. Ycas, F. R. Giorgetta, K. C. Cossel, E. M. Waxman, E. Baumann, N. R. Newbury, and I. Coddington, Optica **6**, 165 (2019).
23. J. Kim and Y. Song, Adv. Opt. Photon. **8**, 465 (2016).
24. L. Nugent-Glandorf, T. A. Johnson, Y. Kobayashi, and S. A. Diddams, Opt. Lett. **36**, 1578 (2011).
25. Y. Liu, D. Luo, C. Wang, Z. Zhu, and W. Li, Laser Phys. **28**, 035106 (2018).
26. N. R. Newbury and W. C. Swann, J. Opt. Soc. Am. B **24**, 1756 (2007).
27. H. Kubota, K. R. Tamura, and M. Nakazawa, J. Opt. Soc. Am. B **16**, 2223 (1999).
28. P. Gierschke, C. Jauregui, T. Gottschall, and J. Limpert, Opt. Express **27**, 17041 (2019).
29. K. L. Corwin, N. R. Newbury, J. M. Dudley, S. Coen, S. A. Diddams, K. Weber, and R. S. Windeler, Phys. Rev. Lett. **90**, 113904 (2003).
30. T. Godin, B. Wetzel, T. Sylvestre, L. Larger, A. Kudlinski, A. Mussot, A. Ben Salem, M. Zghal, G. Genty, F. Dias, and J. M. Dudley, Opt. Express **21**, 18452 (2013).
31. V. Silva de Oliveira, A. Ruehl, P. Masłowski, and I. Hartl, Opt. Lett. **45**, 1914 (2020).